

## Research Article

# Surface Dynamics Transition of Vacuum Vapor Deposited $\text{CH}_3\text{NH}_3\text{PbI}_3$ Perovskite Thin Films

Yunyan Liu <sup>1</sup>, Hongsheng Song,<sup>2</sup> Junshan Xiu,<sup>1</sup> Meiling Sun,<sup>1</sup> Dong Zhao,<sup>1</sup> Zisheng Su <sup>3</sup>, Gongxiang Wei <sup>1</sup> and Fangming Jin<sup>3</sup>

<sup>1</sup>School of Science, Shandong University of Technology, Zibo, Shandong 255049, China

<sup>2</sup>School of Science, Shandong Jianzhu University, Jinan, Shandong 250101, China

<sup>3</sup>State Key Laboratory of Luminescence and Applications, Changchun Institute of Optics, Fine Mechanics and Physics, Chinese Academy of Sciences, Changchun, Jilin 130033, China

Correspondence should be addressed to Zisheng Su; [suzs@ciomp.ac.cn](mailto:suzs@ciomp.ac.cn) and Gongxiang Wei; [weigx@sdut.edu.cn](mailto:weigx@sdut.edu.cn)

Received 30 August 2017; Accepted 4 December 2017; Published 22 February 2018

Academic Editor: Shicai Xu

Copyright © 2018 Yunyan Liu et al. This is an open access article distributed under the Creative Commons Attribution License, which permits unrestricted use, distribution, and reproduction in any medium, provided the original work is properly cited.

The growth dynamics of  $\text{CH}_3\text{NH}_3\text{PbI}_3$  perovskite thin films on ITO covered glass substrate were investigated. The evolution of the film could be divided into two stages. A mound-like surface was obvious at the first stage. Stable dynamic scaling was observed for thicker films at the second stage. Through analyzing the scaling exponent, growth exponent  $\beta$ , and 2D fast Fourier transform, it is concluded that, at the second stage, the growth mechanism of mound formation does not play a major role, and the film growth mechanism can be described by Mullins diffusion equation.

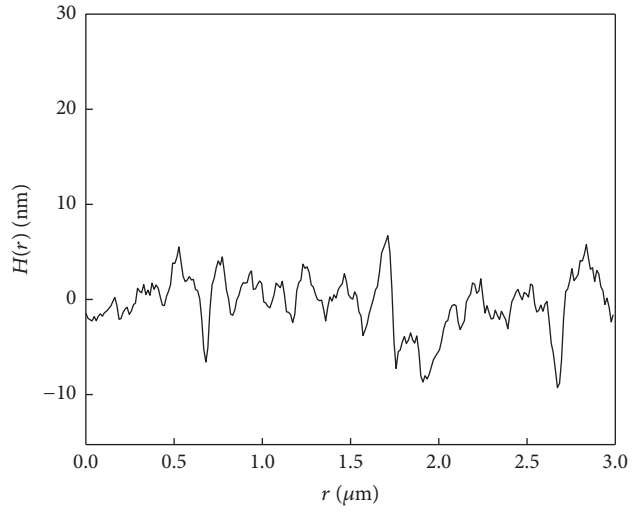
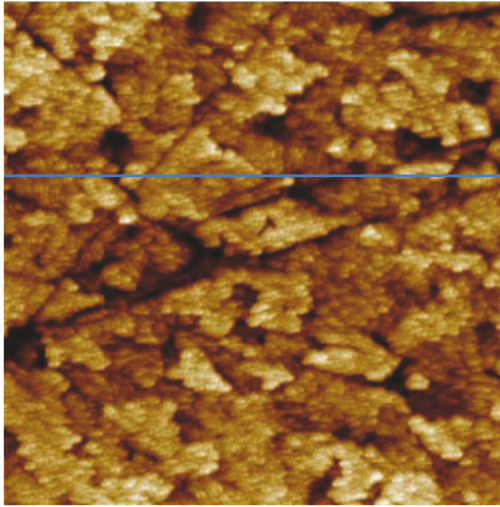
## 1. Introduction

In the past few years, organic–inorganic halide perovskites materials have been intensively investigated for their excellent combination of optoelectronic properties and low cost. Perovskites have found applications in many fields including photovoltaics, lasing, and lighting [1–3] and also potential application in sensitive devices such as photoelectric sensors and gas sensors [4, 5]. The power conversion efficiency (PCE) of perovskite solar cells has increased rapidly from 3.8% to 22.1% in merely 5 years [6–9]. However, the devices' performance and stability are impacted by problems associated with uniformity morphology, coverage, and roughness of the perovskite films. In addition, there is still limited knowledge of the morphology evolution and basic growth dynamics of the halide perovskite thin films.

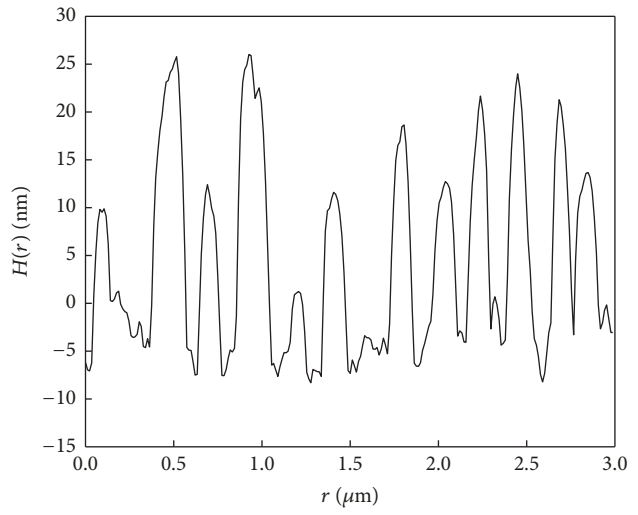
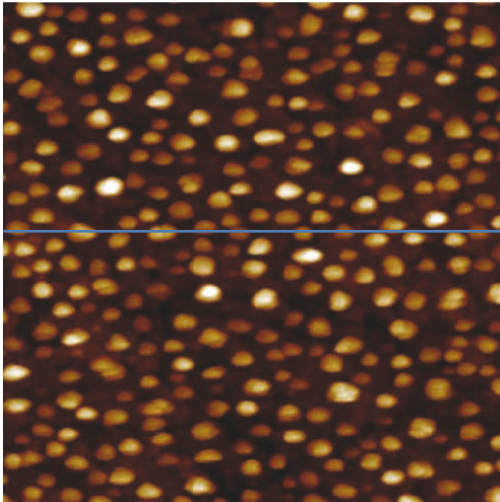
For inorganic and organic thin films, scaling concepts have been developed to quantify the statistical properties of the morphology evolution of the growth front in order to study the growth dynamics of thin films. Various surface growth mechanisms have been supported by different growth models with different sets of scaling exponents [10]. Within

this framework, the growth-induced surface morphology information is described by the equal-time height–height correlation function  $H(r, t)$ .  $H(r, t)$  is defined as a function of lateral position  $r$  and deposition time  $t$  by  $H(r, t) = \langle [h(r, t) - h(0, t)]^2 \rangle$ , where  $h(r, t)$  represents the relative surface height at position  $r$  and time  $t$  with respect to the average surface height  $\langle h(t) \rangle$ .

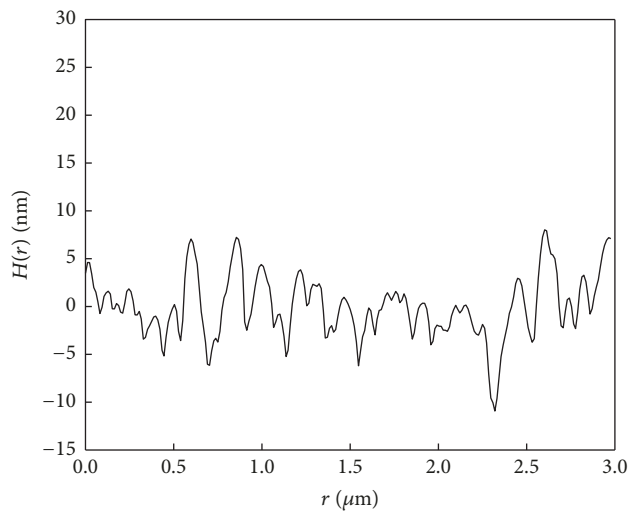
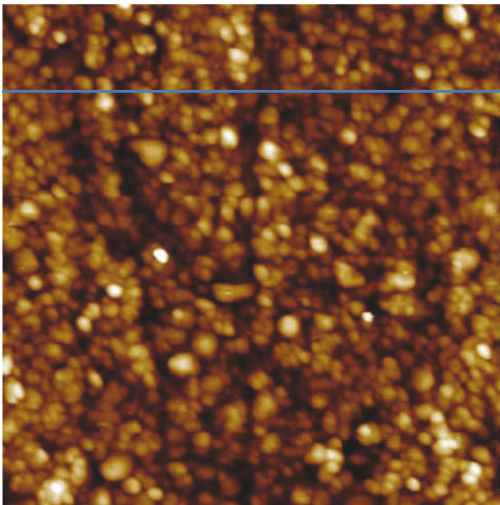
We have reported the scaling behavior and related physical growth dynamics of  $\text{MAPbI}_3$  perovskite thin films on smooth Si substrates [11]. However, practical applications of devices require the perovskite thin films to be deposited on a wide variety of substrates. The nucleation and growth of the deposited perovskite thin films are strongly affected by the surface properties of the substrates underneath the growing films. In this article, the morphology evolution and growth kinetics of  $\text{CH}_3\text{NH}_3\text{PbI}_3$  ( $\text{MAPbI}_3$ ) perovskite thin films by vacuum vapor deposition onto rough ITO covered glass substrates were investigated by analyzing the height–height correlation function  $H(r, t)$ , scaling exponents  $\alpha$ ,  $\beta$ , and  $1/z$ , and 2D fast Fourier transform. The transition in the growth process of thermally evaporated  $\text{MAPbI}_3$  thin films from mound to Mullins growth is found, and this transition



(a)



(b)



(c)

FIGURE 1: Continued.

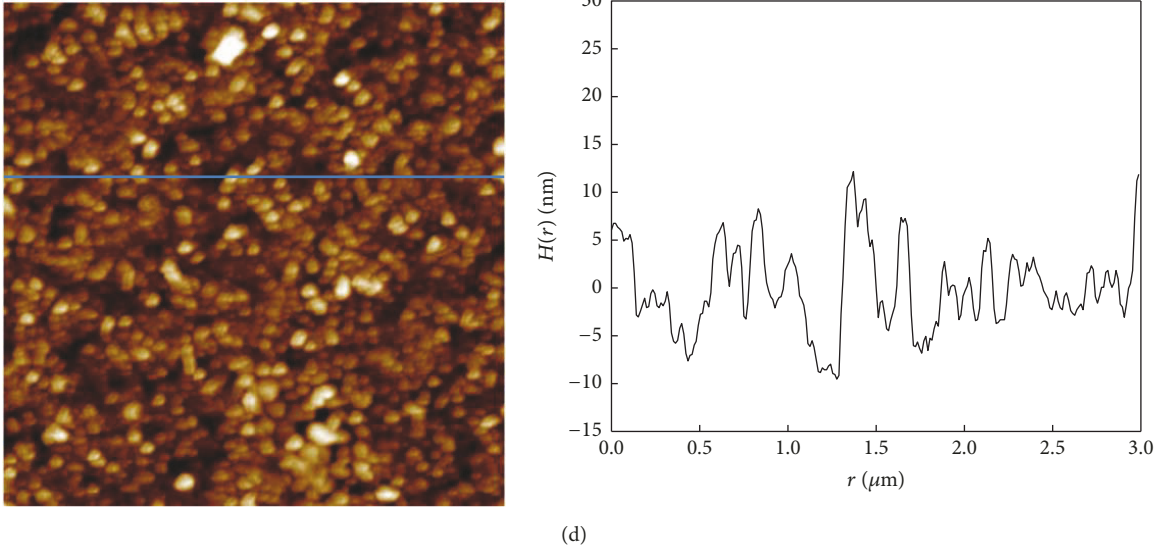


FIGURE 1: Representative AFM images ( $3\ \mu\text{m} \times 3\ \mu\text{m}$ ) and one-dimensional cross-sectional scan of the surface profile of (a) ITO coated glass and MAPbI<sub>3</sub> thin film on ITO coated glass substrates for deposition time of (b) 130, (c) 200, and (d) 500 seconds.

could be resulting from the competition between step-edge bias (SEB) and surface diffusion. This result is quite different from that of Si substrates, which indicates that the perovskite thin films' performance is strongly dependent on the surface properties of the substrates.

## 2. Materials and Methods

The MAPbI<sub>3</sub> perovskite thin films were fabricated by thermal evaporation on ITO (indium tin oxide) covered glass substrates. The substrates were routinely cleaned, followed by UV-ozone treatment for 10 min. The substrates were not intentionally heated during deposition and all the films were not post-heat-treated. The background pressure of the vacuum chamber for thermal evaporation is  $5 \times 10^{-4}$  Pa. The MAPbI<sub>3</sub> film was grown by thermally coevaporating CH<sub>3</sub>NH<sub>3</sub>I and PbI<sub>2</sub> with a mass ratio of CH<sub>3</sub>NH<sub>3</sub>I to PbI<sub>2</sub> of 4:1. The growth rate was kept at 0.5 Å/s for MAPbI<sub>3</sub> films. The perovskite layer thicknesses from 6.5 to 300 nm were controlled by the deposition time between 130 s and 600 s, respectively. The deposition rate and layer thickness were monitored in situ using oscillating quartz monitors.

The surface topographies were imaged with a Bruker Multimode 8 atomic force microscope (AFM) in tapping mode under ambient air. The scanning area for AFM imaging is  $3\ \mu\text{m} \times 3\ \mu\text{m}$  with a resolution of  $256 \times 256$ . In order to get better statistical properties, repeated measurements were carried out to obtain the average  $H(r, t)$ .

## 3. Results and Discussion

Figures 1(a)–1(d) describe AFM images of the ITO substrate and different MAPbI<sub>3</sub> perovskite thin films of growth time of 130 s, 200 s, and 500 s, respectively. The corresponding 1D

cross-sectional scans of surface profile are also shown, where  $H(r)$  denotes the relative surface height at coordinate  $r$  on the cross section line. The MAPbI<sub>3</sub> film with a deposition time of 130 s shows a dramatically different surface morphology (Figure 1(b)) from that of the ITO substrate (Figure 1(a)). The ITO grooves surface is covered by isolated spherical grains, suggesting the island film growth of perovskite thin films. When growth time  $t \geq 200$  s (Figures 1(c) and 1(d)), the topography of the substrate is invisible and a continuous grainy surface of MAPbI<sub>3</sub> film develops. From the beginning of deposition, as shown in 1D cross-sectional scans of the surface profile, the relative surface height decreases with the increasing deposition time. After a continuous film is formed, the transition of morphology is accompanied by the height increase as more materials are deposited. This indicates that the surface formation evolves from a dynamic smoothing process to a roughening growth, as will be further discussed in the following sections.

For the calculated results of  $w$  and  $\xi$  and scaling exponents  $\alpha \sim 0.83$ ,  $\beta = 0.28 \pm 0.02$ , and  $1/z = 0.26 \pm 0.04$ , refer to [11].

Figure 2 shows the roughness exponent  $\alpha$  as a function of growth time  $t$ . It can be seen that the changes of the variables  $\alpha$  and  $t$  can be divided into two stages. At the first stage ( $t < 200$  s),  $\alpha$  values decrease from about 0.9 to 0.84 with increasing time  $t$ . This implies a strong interaction between the incoming flux and the substrates at the initial coverage stage, and the surface experiences an unstable scaling behavior [12]. At the second stage ( $t \geq 200$  s),  $\alpha$  values are almost invariant and the average value is about 0.83. This indicates the stable kinetic roughening corresponding to continuous film growth at this stage [13].

The calculated scaling exponent  $\alpha$  at the first stage is quite close to the one predicted by the model of mound formation or Mullins model where, in both cases,  $\alpha = 1$ . However, it may be smaller than that predicted by the theoretical model

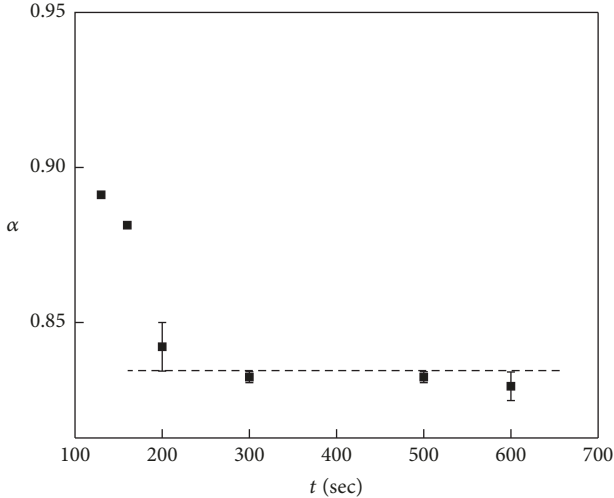


FIGURE 2: The roughness exponent  $\alpha$  as a function of growth time  $t$  for MAPbI<sub>3</sub> thin films; the short dashed line shows the average value of  $\alpha$  when  $t \geq 200$  s.

practically, for example, SnCl<sub>2</sub>Pc on glass ( $\alpha = 0.9$ ) [14]. The mound growth mechanism can usually occur in thin film growth in the presence of nonlocal roughening effects such as shadowing or step-edge barrier (Schwoebel barrier), which is associated with reduced interlayer transport [15, 16]. Mullins growth refers to a linear model of a self-affine growth mechanism, in which the growth is dominated by the surface diffusion, and in turn the latter is due to the curvature induced chemical potential gradient. The ring structure is the main feature of SEB induced mound growth [17]. We have plotted 2D fast Fourier transform (FFT) of the surface from the AFM images (Figures 3(a)–3(d)), and the formation of the mound at the initial film growth stage is supported by the ring-like behavior in the 2D FFT of the film for growth time of less than 200 s (Figure 3(a)). Furthermore, the mound surface is supported by the  $H(r, t)$  curves displaying an overshoot in the crossover [15] and by the oscillation in larger  $r$  as shown in the curves of  $t < 200$  s in [11]. Hence, the growth of MAPbI<sub>3</sub> film at the first stage is more likely to be governed by SEB induced mound growth model.

For the SEB induced surface, the mound growth model can be described by the following equation:

$$\left( \frac{\partial h}{\partial t} = -\nu \nabla^2 h - k \nabla^4 h + \eta \right). \quad (1)$$

Here,  $\nu$  and  $k$  terms refer to SEB effect and surface diffusion, respectively. Small  $k/\nu$  ratio means that the SEB dominates the growth and the ring structure would be obvious. On the other hand, when  $k/\nu$  is much larger than 1, either SEB is small or surface diffusion is fast, and the ring structure would be beyond recognition [18].

Figure 4(a) shows the log  $w$ -log  $t$  plot. It is clearly shown that  $w$  decreases ( $t < 200$  s) and then increases with time ( $t \geq 200$  s), indicating a shift from smoothing to roughening of film surface. This is consistent with the fluctuation of height as revealed in Figure 1. The solid line in Figure 4(a) is the

linear fit to the data for the second growth stage ( $t \geq 200$  s), when continuous film growth and stable scaling behavior occur, and  $\beta$  is obtained.

$\beta = 0.28 \pm 0.02$  is close to the reported results of vapor deposited oligomer films on silicon substrate ( $\beta = 0.28 \pm 0.05$ ) [19] and recent reports of vapor phase deposition of poly(ethylene) ( $\beta$  varying from 0.20 to 0.33 in postaggregation and aggregation regime, resp.) [20]. Previous theoretical or experimental studies have revealed that, in the step-edge barrier or shadowing effect governing film growth, the value of  $\beta$  will be equal to or greater than 0.5 [21, 22]. Our  $\beta$  value of about 0.28 indicates that both step-edge barrier and shadowing effects are weak during the growth of perovskite films at the second stage, and this may lead to the situation of  $k/\nu \gg 1$  as discussed in (1). In this case, the satellite ring structure should not be observed for the films of the second stage. To confirm this, we investigated the ring structure for the MAPbI<sub>3</sub> films. Results show that the ring structure gradually disappears and could not be definitely determined for  $t \geq 200$  s as expected, as shown in Figures 3(b)–3(d). This information reveals that the surface diffusion induced growth, instead of mound growth, might be the dominant mechanism at the second stage. It should be noted that the value of growth exponent  $\beta = 0.28 \pm 0.02$  is close to the predictions of the surface diffusion induced Mullins scenario ( $\beta \approx 0.25$ ) or Kardar–Parisi–Zhang (KPZ) model ( $\beta \approx 0.24$ ) [23]. However, KPZ type of growth develops the scaling exponent  $\alpha \approx 0.38$ , and it is well below  $\alpha \approx 0.83$  as obtained at the second growth stage in our work; thus, KPZ growth is excluded. In fact,  $\alpha \approx 0.83$  is in the range of the prediction of the surface diffusion mechanism ( $0.66 \leq \alpha \leq 1$ ) [24]. These results strongly support the fact that surface diffusion dominated growth offers a more plausible scenario than others at the second growth stage of MAPbI<sub>3</sub> thin films. In this case, the  $\nu$  terms could be neglected from (1), and the growth at the second stage would be governed by Mullins diffusion described by the following [25]:

$$\left( \frac{\partial h}{\partial t} = -k \nabla^4 h + \eta \right). \quad (2)$$

The dominant growth mechanism might shift from SEB induced mound growth at the first growth stage to surface diffusion induced Mullins growth at the second stage.

The correlation length  $\xi$  at each growth time could be determined by fitting the curve of  $H(r)$  to the phenomenological function for self-affine proposition by Sinha et al. [26]:

$$H(r) = 2w^2 \left( 1 - \exp \left( - \left( \frac{r}{\xi} \right)^{2\alpha} \right) \right). \quad (3)$$

Figure 4(b) displays the log-log plot of  $\xi$  versus  $t$ . The solid line in Figure 4(b) is the linear fit to the data for the second growth stage ( $t \geq 200$  s), and  $1/z$  is obtained.  $1/z = 0.26 \pm 0.04$  is a little lower than  $\beta/\alpha \approx 0.33$ . This may indicate weak anomalous scaling, where the local slope is no longer time-independent for short range of  $r$  and corresponding growth is not stationary. This supports the nonstationary growth behavior of short range  $H(r)$  as revealed in [11].

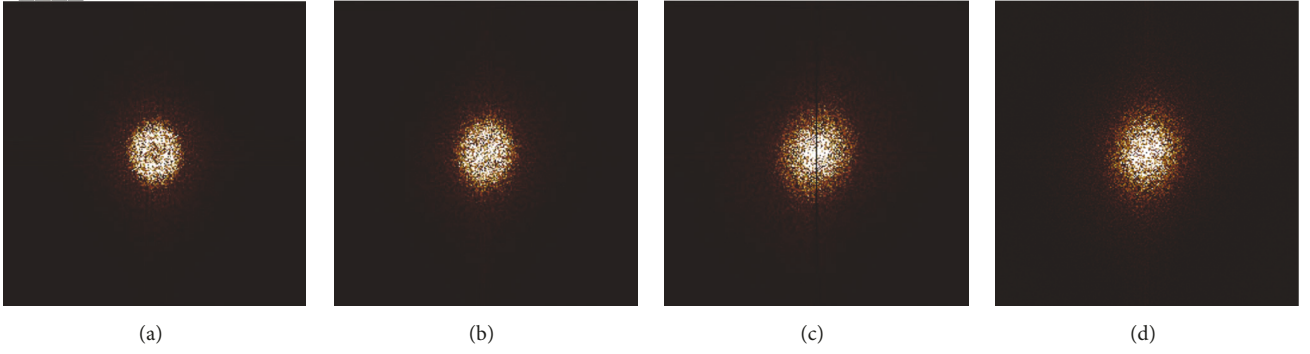


FIGURE 3: 2D FFT of the surface from MAPbI<sub>3</sub> thin film AFM images of deposition time of (a) 130 s, (b) 160 s, (c) 500 s, and (d) 600 s.

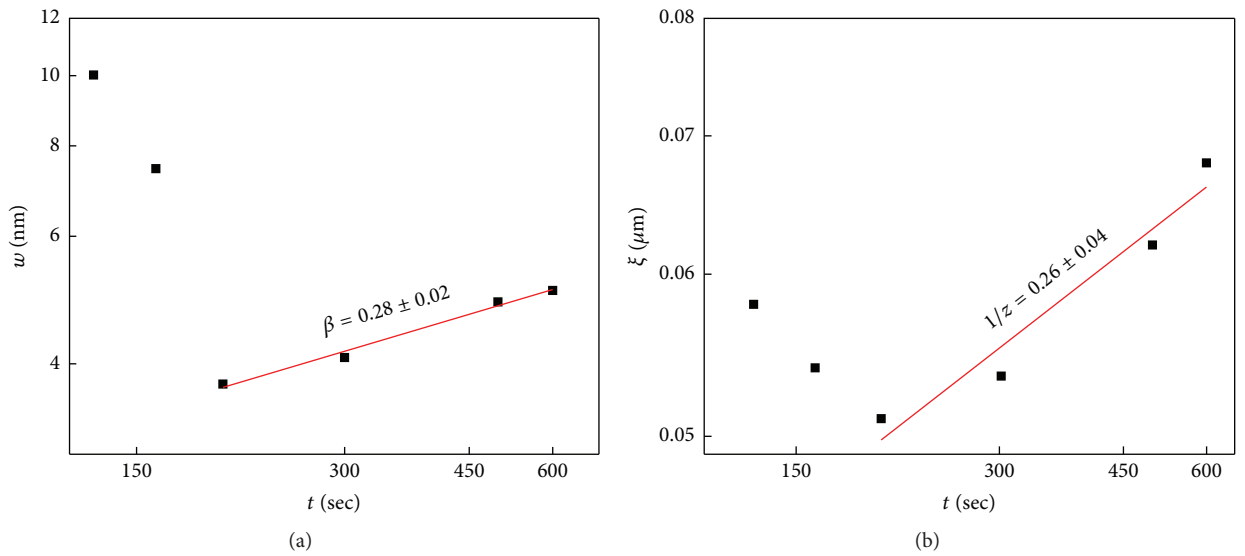


FIGURE 4: The log-log plot of (a)  $w$  and (b)  $\xi$  as a function of growth time  $t$  for MAPbI<sub>3</sub> thin films. The solid lines are linear fits to the data for growth time  $t \geq 200$  s which give  $\beta = 0.28 \pm 0.02$  and  $1/z = 0.26 \pm 0.04$ .

We note that the interface width  $w$  decreases with time at early growth time. This phenomenon is in contrast to the results obtained in theoretical prediction and most experiments show that the surface roughness evolves with time in the form of power law as  $w(t) \propto t^\beta$  at the initial film growth stage, where ideal smooth substrate surfaces are applied. However, smoothing may occur at the initial film growth due to the complicated growth conditions in real systems [27], which have drawn little attention in the past few years. Previously, studies revealed some smoothing mechanisms of various films, including rough substrate, surface diffusion, step-edge barrier effect, nonlinearity, or reemission [27–30]. The surface smoothing in the initial growth of ZrO<sub>2</sub> thin films deposited on glass, because of the interaction of substrate and diffusion of deposited atoms, has been reported [28]. Ballestad et al. [29] explained the mounded surface smoothing using nonlinear Kardar–Parisi–Zhang (KPZ) equation ( $\partial h/\partial t = \nu \nabla^2 h + (\lambda/2)(\nabla h)^2 + \eta$ ). Liu et al. [30] observed linear surface smoothing which could be explained by noise driven Mullins diffusion equation

( $\partial h/\partial t = -k \nabla^4 h + \eta$ ). Also, an example can be found in [27], from kinetic Monte Carlo (KMC) simulations, where the initial smoothing effect of InAs films on InAs substrates is attributed to the presence of an asymmetric step-edge barrier induced linear instability.

Due to the step-edge barrier at the early growth stage of the MAPbI<sub>3</sub> film, which prevents atoms from hopping from the top of the island to the substrate, the adatoms are more apt to combine with each other than with the substrate, and this leads to the initial mound growth. The isolated island has not completely covered the substrate and the height difference between the island and the substrate was explained as a possible origin for the initial larger roughness ( $w$ ) of the surface. At the same time, deposited atoms prefer to move downward by overcoming the island edge barrier to minimize the surface energy. As more islands grow and merge with each other, the surface of the substrates is gradually covered by more and more film. The height difference between the newly formed islands, merged islands, and the ITO substrates gradually decreases. This decrease will continue until the roughness

fluctuation of homogeneous film morphology becomes evident, due to growth behaviors of the continuous MAPbI<sub>3</sub> thin films, and  $w$  evolves with time in the form of power law as  $w(t) \propto t^\beta$ . On the other hand, the introduction of newly built grain boundary and in-plane tensile stress in merged islands and continuous film grains could change the behavior during film growth [31]. In such case, the film growth evolves into a different evolution mechanism which should be dominated by a weak step-edge barrier and large surface diffusion at the second stage. The variations of the growth mechanism may also be considered to be related to thickness dependent structural changes or molecular reorientation [21, 32], ultimately leading to the morphology evolution of thin films.

#### 4. Conclusions

In conclusion, the growth dynamics of MAPbI<sub>3</sub> thin films by thermal evaporation on rough ITO substrates were investigated. Two growth stages can be found before and after the formation of continuous films. By analyzing the scaling behavior of the films and 2D fast Fourier transform, we conclude that step-edge barriers governing growth result in the morphology evolution of MAPbI<sub>3</sub> thin films following obvious mound-like formation at the initial growth stage. At the second stage, stable kinetic roughening corresponds to a continuous film growth, with  $\alpha \approx 0.83$ , growth exponent  $\beta = 0.28 \pm 0.02$ , and a dynamic exponent  $1/z = 0.26 \pm 0.04$ . The mound feature disappeared and the film growth at the second stage was shown to belong to a Mullins diffusion model, and the dominant roughening mechanism would be diffusion induced dynamic growth. The shift of the interface width  $w$  from a decrease to an increase also suggests different evolution mechanisms at different growth stages. The nonstationary growth behavior of short range  $H(r)$  and the relation of  $1/z \neq \beta/\alpha$  indicate the anomalous scaling behavior of MAPbI<sub>3</sub> surface evolution.

#### Conflicts of Interest

The authors declare that they have no conflicts of interest.

#### Acknowledgments

The authors acknowledge the support of the National Natural Science Foundation of China (11404191, 61604149, and 11574185) and Shandong Provincial Natural Science Foundation (ZR2016AQ22). This work is also supported by the Program for the Top Young of SDUT, China.

#### References

- [1] M. Liu, M. B. Johnston, and H. J. Snaith, "Efficient planar heterojunction perovskite solar cells by vapour deposition," *Nature*, vol. 501, no. 7467, pp. 395–398, 2013.
- [2] F. Deschler, M. Price, S. Pathak et al., "High photoluminescence efficiency and optically pumped lasing in solution-processed mixed halide perovskite semiconductors," *The Journal of Physical Chemistry Letters*, vol. 5, no. 8, pp. 1421–1426, 2014.
- [3] Z.-K. Tan, R. S. Moghaddam, M. L. Lai et al., "Bright light-emitting diodes based on organometal halide perovskite," *Nature Nanotechnology*, vol. 9, no. 9, pp. 687–692, 2014.
- [4] L. T. Dou, Y. M. Yang, J. B. You et al., "Solution-processed hybrid perovskite photodetectors with high detectivity," *Nature Communications*, vol. 5, article 6404, 2014.
- [5] H. J. Jin, Y. Li, Y. Zeng, Z. Q. Hua, and H. M. Tian, "Sensitive characteristics of the sensitive devices prepared by WO<sub>3</sub> and CH<sub>3</sub>NH<sub>3</sub>PbI<sub>3</sub> perovskite," *Micronanoelectronic Technology*, vol. 54, p. 101, 2017 (Chinese).
- [6] A. Kojima, K. Teshima, Y. Shirai, and T. Miyasaka, "Organometal halide perovskites as visible-light sensitizers for photovoltaic cells," *Journal of the American Chemical Society*, vol. 131, no. 17, pp. 6050–6051, 2009.
- [7] H.-S. Kim, C.-R. Lee, J.-H. Im et al., "Lead iodide perovskite sensitized all-solid-state submicron thin film mesoscopic solar cell with efficiency exceeding 9%," *Scientific Reports*, vol. 2, article 591, 2012.
- [8] J. Burschka, N. Pellet, S. Moon et al., "Sequential deposition as a route to high-performance perovskite-sensitized solar cells," *Nature*, vol. 499, no. 7458, pp. 316–319, 2013.
- [9] Research Cell Efficiency Records, National Renewable Energy Laboratory, <http://www.nrel.gov/ncpv>.
- [10] P. Meakin, *Fractals, Scaling and Growth Far from Equilibrium*, Cambridge University Press, New York, NY, USA, 1998.
- [11] Y. Y. Liu, T. Zhou, M. L. Sun et al., "Scaling behavior and morphology evolution of CH<sub>3</sub>NH<sub>3</sub>PbI<sub>3</sub> perovskite thin films grown by thermal evaporation," *Materials Research Express*, vol. 4, no. 7, Article ID 075510, 2017.
- [12] S. Zorba, L. Yan, N. J. Watkins, and Y. Gao, "Kinetic roughening study of perylene on glass and Au substrates," *Applied Physics Letters*, vol. 81, no. 27, pp. 5195–5198, 2002.
- [13] J. J. Yang, J. Tang, N. Liu, F. Ma, W. Tang, and K. W. Xu, "Unstable kinetic roughening during the island coalescence stage of sputtered tantalum films," *Journal of Applied Physics*, vol. 111, no. 10, Article ID 104303, pp. 1–5, 2012.
- [14] S. M. Obaidulla and P. K. Giri, "Surface roughening and scaling behavior of vacuum-deposited SnCl<sub>2</sub>Pc organic thin films on different substrates," *Applied Physics Letters*, vol. 107, no. 22, Article ID 221910, 2015.
- [15] J. H. Yao and H. Guo, "Shadowing instability in three dimensions," *Physical Review E: Statistical Physics, Plasmas, Fluids, and Related Interdisciplinary Topics*, vol. 47, no. 2, pp. 1007–1011, 1993.
- [16] M. D. Johnson, C. Orme, A. W. Hunt et al., "Stable and unstable growth in molecular beam epitaxy," *Physical Review Letters*, vol. 72, no. 1, pp. 116–119, 1994.
- [17] Y. P. Zhao, H. N. Yang, G. C. Wang, and T. M. Lu, "Diffraction from diffusion-barrier-induced mound structures in epitaxial growth fronts," *Physical Review B: Condensed Matter and Materials Physics*, vol. 57, no. 3, pp. 1922–1934, 1998.
- [18] Y. P. Zhao, G. C. Wang, and T. M. Lu, *Characterization of Amorphous and Crystalline Rough Surface: Principles and Applications*, vol. 37, Academic Press, New York, NY, USA, 2001.
- [19] D. Tsamouras, G. Palasantzas, and J. Th. M. De Hosson, "Growth front roughening of room-temperature deposited oligomer films," *Applied Physics Letters*, vol. 79, no. 12, pp. 1801–1803, 2001.
- [20] A. Choukurov, I. Melnichuk, I. Gordeev et al., "Dynamic scaling and kinetic roughening of poly(ethylene) islands grown

- by vapor phase deposition,” *Thin Solid Films*, vol. 565, pp. 249–260, 2014.
- [21] G. Hlawacek, P. Puschnig, P. Frank, A. Winkler, C. Ambrosch-Drax, and C. Teichert, “Characterization of step-edge barriers in organic thin-film growth,” *Science*, vol. 321, no. 5885, pp. 108–111, 2008.
- [22] J. Yu and J. G. Amar, “Dynamical scaling behavior in two-dimensional ballistic deposition with shadowing,” *Physical Review E: Statistical, Nonlinear, and Soft Matter Physics*, vol. 66, no. 2, Article ID 021603, 2002.
- [23] M. Kardar, G. Parisi, and Y.-C. Zhang, “Dynamic scaling of growing interfaces,” *Physical Review Letters*, vol. 56, no. 9, pp. 889–892, 1986.
- [24] Z.-W. Lai and S. Das Sarma, “Kinetic growth with surface relaxation: Continuum versus atomistic models,” *Physical Review Letters*, vol. 66, no. 18, pp. 2348–2351, 1991.
- [25] W. W. Mullins, “Theory of thermal grooving,” *Journal of Applied Physics*, vol. 28, no. 3, pp. 333–339, 1957.
- [26] S. K. Sinha, E. B. Sirota, S. Garoff, and H. B. Stanley, “X-ray and neutron scattering from rough surfaces,” *Physical Review B: Condensed Matter and Materials Physics*, vol. 38, no. 4, pp. 2297–2311, 1988.
- [27] M. F. Gyure, J. J. Zinck, C. Ratsch, and D. D. Vvedensky, “Unstable growth on rough surfaces,” *Physical Review Letters*, vol. 81, no. 22, pp. 4931–4934, 1998.
- [28] H. J. Qi, L. H. Huang, Z. S. Tang, C. F. Cheng, J. D. Shao, and Z. X. Fan, “Roughness evolution of  $\text{ZrO}_2$  thin films grown by reactive ion beam sputtering,” *Thin Solid Films*, vol. 444, no. 1-2, pp. 146–152, 2003.
- [29] A. Ballestad, B. J. Ruck, M. Adamcyk, T. Pinnington, and T. Tiedje, “Evidence from the surface morphology for nonlinear growth of epitaxial GaAs films,” *Physical Review Letters*, vol. 86, no. 11, pp. 2377–2380, 2001.
- [30] Z.-J. Liu, P. W. Shum, and Y. G. Shen, “Linear surface smoothening of  $(\text{Ti}_{0.48}\text{Al}_{0.52})\text{N}$  thin films grown on rough substrates,” *Applied Physics Letters*, vol. 86, no. 25, Article ID 251908, pp. 1–3, 2005.
- [31] C. Friesen, S. C. Seel, and C. V. Thompson, “Reversible stress changes at all stages of Volmer-Weber film growth,” *Journal of Applied Physics*, vol. 95, no. 3, pp. 1011–1020, 2004.
- [32] Y. Zhang, E. Barrena, X. Zhang, A. Turak, F. Maye, and H. Dosch, “New insight into the role of the interfacial molecular structure on growth and scaling in organic heterostructures,” *The Journal of Physical Chemistry C*, vol. 114, no. 32, pp. 13752–13758, 2010.



Hindawi

Submit your manuscripts at  
[www.hindawi.com](http://www.hindawi.com)

